PCCP

Reaction kinetics of O(^{1}D) with CF$_3$CN

Mitsuhiko Kono† and Yutaka Matsumi*

Solar-Terrestrial Environment Laboratory, Nagoya University, Honohara 3-13, Toyokawa, Aichi, 442-8507, Japan. E-mail: matsumi@stelab.nagoya-u.ac.jp

Received 4th September 2000, Accepted 26th October 2000
First published as an Advance Article on the web 22nd November 2000

The rate constant for removal of O(^{1}D) by reaction with CF$_3$CN has been measured to be $(1.3 \pm 0.2) \times 10^{-10}$ cm^3 molecule^{-1} s^{-1} at room temperature by a time-resolved laser induced fluorescence (LIF) technique. The quantum yield for the electronic quenching O(^{1}D) to O(^{3}P) has been also measured to be 0.14 ± 0.02. The O(^{1}D) and O(^{3}P) atoms were detected by LIF using a vacuum ultraviolet laser as a probe laser. CN(X $^2\Sigma^+$) and NCO(X $^2\Pi$) products were also detected by LIF using ultraviolet and visible lasers, respectively. The CN(X) radical was observed as a primary product, while the NCO(X $^2\Pi$) radical was not observed as a primary product in the present reaction.

1. Introduction

Reactions of electronically excited oxygen atoms O(^{1}D) are a significant chemical channel for the removal of the mixed halogenated methane derivatives CF$_n$X$_{4-n}$ (X = Cl, Br, I) in the stratosphere.[1–4] The kinetics for the production of O(^{3}P), ClO and Cl radicals following the O(^{1}D) reaction with the chlorofluoromethane CF$_n$Cl$_{4-n}$ (CFC-1*n*) have been well determined,[5,6] because it is important to estimate the production rate of ClO$_x$ destroying the ozone layer.[7–9] The dominant pathways of these reactions are the production of O(^{3}P) and ClO, while the reaction channel of Cl production is a quite small contribution.[5] It is interesting that the Cl atom is hardly produced in the reaction CF$_3$Cl + O(^{1}D) in spite of the largest reaction energy released. The reason for this phenomenon is not yet understood.

To examine whether similar phenomena are observed in the reaction of other species, we investigated the reaction of O(^{1}D) with CF$_3$CN which was used as a pseudo-CF$_3$Cl molecule. The electronic quenching reaction channels to produce O(^{3}P) are

$$\mathrm{CF_3CN + O(^1D)}$$
$$\rightarrow \mathrm{CF_3CN + O(^3P)}; \qquad -\Delta H = 190\ \mathrm{kJ\ mol^{-1}}, \quad (1)$$
$$\rightarrow \mathrm{CF_3NC + O(^3P)}; \qquad -\Delta H = 143\ \mathrm{kJ\ mol^{-1}}, \quad (2)$$

where ΔH is the standard enthalpy of reaction at 298 K.[10] The possible spin-allowed reaction channels are

$$\mathrm{CF_3CN + O(^1D)}$$
$$\rightarrow \mathrm{CF_3 + NCO(X\,^2\Pi)}; \qquad -\Delta H = 333\ \mathrm{kJ\ mol^{-1}}, \quad (3)$$
$$\rightarrow \mathrm{CF_3 + NCO(A\,^2\Sigma^+)}; \qquad -\Delta H = 61\ \mathrm{kJ\ mol^{-1}}, \quad (4)$$
$$\rightarrow \mathrm{CF_3 + CNO(X\,^2\Pi)}; \qquad -\Delta H = 72\ \mathrm{kJ\ mol^{-1}}, \quad (5)$$
$$\rightarrow \mathrm{CF_3C + NO(X\,^2\Pi)}; \qquad -\Delta H \approx 0\ \mathrm{kJ\ mol^{-1}} \quad (6)$$
$$\rightarrow \mathrm{CF_3O + CN(X\,^2\Sigma^+)}; \qquad -\Delta H = 168\ \mathrm{kJ\ mol^{-1}}, \quad (7)$$
$$\rightarrow \mathrm{CF_3O + CN(A\,^2\Pi)}; \qquad -\Delta H = 59\ \mathrm{kJ\ mol^{-1}}. \quad (8)$$

In the present study, the decay of O(^{1}D) and rise of O(^{3}P) were monitored to measure the total reaction rate constant, k_{total}. The signal of O(^{1}D) was detected by LIF using a tunable vacuum ultraviolet (VUV) laser. The O(^{3}P), CN(X) and NCO(X) radical products are also detected by LIF using VUV, UV and VIS lasers, respectively. The quantum yield of the quenching reaction, ϕ_{q}, was measured by comparison between the O(^{3}P) signal intensity formed in the present reaction and that in the quenching reaction

$$\mathrm{N_2 + O(^1D) \rightarrow N_2 + O(^3P)}, \qquad (9)$$

in which the quantum yield is defined as unity.[11] From the observed quenching rate constant, $k_{\mathrm{q}} = k_{\mathrm{total}}\phi_{\mathrm{q}}$, and the time profile of the LIF signals of CN(X) and NCO(X), the reaction mechanism is discussed.

2. Experimental

The experimental setup was essentially the same as in the previous studies.[12] The reaction cell ($60 \times 60 \times 60$ mm^3) was evacuated by a rotary pump through a liquid-N$_2$ trap. Sample gas mixtures containing N$_2$O as an O(^{1}D) source, CF$_3$CN or N$_2$ as a reactant, and He as a buffer were flowed slowly through the reaction cell where the pressure was measured by a Baratron gauge. The N$_2$O, CF$_3$CN, N$_2$ and He gases were obtained commercially and used without further purification. The O(^{1}D) was generated in the reaction cell by the photolysis of N$_2$O at 193 nm using an ArF laser (Lambda Physik, Compex; 50 mJ). The initial concentration of O(^{1}D) is estimated to be $\sim 10^9$ molecule cm^{-3}. Because translationally hot O(^{1}D) atoms are thermalized rapidly by collisions with buffer gas,[13] the hot atom effect can be ignored under the present experimental conditions. The probe laser beam for the detection of O(^{1}D) or reaction products was also introduced in the reaction cell after the delay. The reaction time is defined as this delay time, *t*, between the photolysis and probe laser pulses, which is controlled by a pulse generator (Stanford Research Systems, DG535).

The O(^{1}D) and O(^{3}P$_2$) atoms were detected by LIF for the 3s ^{1}D°–2p ^{1}D transition at 115.22 nm and 3s ^{3}S°–2p ^{3}P$_2$ transition at 130.22 nm, respectively. The VUV wavelengths of 115.22 and 130.22 nm were generated by frequency tripling (3ω) of a dye laser (Lambda Physik, FL3002, 5 mJ pulse^{-1}) at 345.6 nm in Xe (50 Torr) and Ar (150 Torr) gas mixture and

---

† Present address: Atomic and Molecular Physics Laboratory, Research School of Physical Sciences and Engineering, The Australian National University, Canberra, ACT 0200, Australia.

DOI: 10.1039/b007199o

by four-wave difference mixing ($2\omega_1$–ω_2) using two dye lasers (Lambda Physik, FL3002 and Scanmate) in Kr gas (20 Torr), respectively. The dye laser output was frequency doubled by a BBO crystal for the ω_1 light of wavelength 212.56 nm, which was two-photon resonant with Kr $5p[1/2]_0$. The dye lasers were pumped by a XeCl excimer laser (Lambda Physik, Lextra-50). The wavelength of ω_2 was tuned around 578.1 nm. The laser beams were focused into a Xe or Kr gas cell by a lens with a focal length of 200 mm. The VUV light generated in the Xe or Kr gas cell was introduced into the reaction cell through a LiF window in a direction orthogonal to the photolysis laser direction. The intensity of the VUV beam was monitored by the photo-current measurement in an NO ionization cell located behind the reaction cell. The resonant LIF signal was detected by a photomultiplier tube (EMR, Model 547J-08-17) at right angles to both the photolysis and probe laser beams.

The CN($X\,^2\Sigma^+$) and NCO($X\,^2\Pi$) radicals were also detected by LIF for the CN($B\,^2\Sigma^+$–$X\,^2\Sigma^+$) transition around 390 nm and NCO($A\,^2\Sigma^+$–$X\,^2\Pi$) transition around 440 nm, respectively, using the dye laser (Lambda Physik, FL3002) pumped by the XeCl excimer laser (Lambda, Lextra-50). The UV (390 nm) or VIS (440 nm) probe laser beam was introduced into the reaction cell in a direction counter-propagated to the photolysis laser beam. The intensities of the UV and VIS beams were monitored by a photodiode. LIF signals of CN(B–X) and NCO(A–X) transitions were detected by a dynode-gated photomultiplier tube (Hamamatsu, 1P28 and C1392-56) with a high speed amplifier (Hamamatsu C5594) to separate the resonance fluorescence and the strong laser scattering.

3. Results

3.1. Total rate constant for the removal of O(^{1}D)

The temporal profiles of O(^{1}D) and O(^{3}P) were recorded in order to measure the total reaction rate constant. Fig. 1 shows the temporal profile of O(^{1}D) obtained when the pressures of N_2O, CF_3CN and He are 2.3, 23 and 455 mTorr, respectively. Fig. 2 shows the temporal profile of O(^{3}P) obtained when the pressures of N_2O, CF_3CN and He are 9, 91 and 1900 mTorr, respectively. These conditions were limited by a certain concentration of N_2O needed in order to see the signal and therefore they needed high concentrations of CF_3CN to ensure the dominance of the target reaction. The diffusion of the O(^{1}D) atoms from the viewing zone could be ignored in the O(^{1}D) decay measurements, since the diffusion rate was measured by the decay profile of O(^{3}P) signal to be ~0.01 μs^{-1} at the cell pressure of 500 mTorr. To avoid hot atom effects due to the excess energy in the photodissociation of N_2O, the data at the delay time between 0 and 1 μs were excluded in the calculations of the decay and rise rates. It can be estimated that the intramultiplet relaxation among the spin–orbit states of O(^3P_j) to the thermal distribution is accomplished within 1 μs at the pressure of 2 Torr, based on the report of the intramultiplet relaxation with collisions with various molecules.[12] Therefore, the distributions among the spin–orbit states $j = 2$, 1 and 0 of O(^3P_j) should be entirely thermalized under the present experimental conditions and the measured O($^3P_2$) signal intensity is proportional to the total concentration of spin–orbit states of O(^{3}P). The thermal population at room temperature is $[O(^3P_2)] : [O(^3P_1)] : [O(^3P_0)] = 1 : 0.282 : 0.068$.

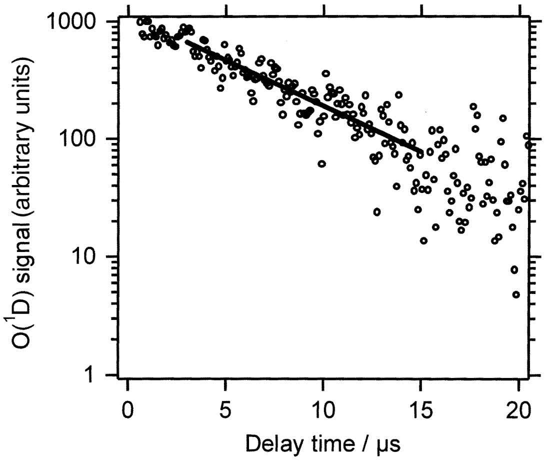

Fig. 1 Temporal profile of O(^{1}D) obtained in the reaction between O(^{1}D) produced from the photolysis of N_2O at 193 nm and CF_3CN. The pressures of N_2O, CF_3CN and He are 2.3, 23 and 455 mTorr, respectively. The horizontal scale is the delay time between photolysis and probe laser pulses. The solid line is the least-squares fit to the observed profile by the exponential decay function.

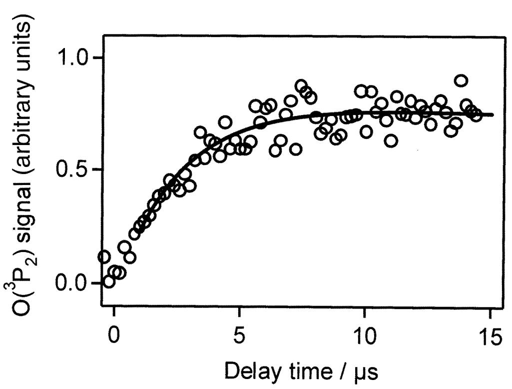

Fig. 2 Temporal profile of O($^3P_2$) obtained in the reaction between O(^{1}D) produced from the photolysis of N_2O at 193 nm and CF_3CN. The pressures of N_2O, CF_3CN and He are 9, 91 and 1900 mTorr, respectively. The horizontal scale is the delay time between photolysis and probe laser pulses. The solid line is the least-squares fit to the observed profile by the exponential rise function.

Since the quenching rate constant between O(^{1}D) and He is extremely small ($<5 \times 10^{-14}$ cm^3 molecule^{-1} s^{-1}),[14] the quenching of O(^{1}D) by He can be neglected here. The formation and decay time constants, k(s^{-1}), obtained by the least-squares fit were measured at different pressures in the reaction cell, because they are the function of reactant concentrations, *i.e.*

$$k = k_{N_2O}[N_2O] + k_{CF_3CN}[CF_3CN], \qquad (10)$$

where k_{N_2O} and k_{CF_3CN} are the rate constants for the removal of O(^{1}D) by the reactants N_2O and CF_3CN, respectively, and $[N_2O]$ and $[CF_3CN]$ are the concentrations of N_2O and CF_3CN, respectively. The removal by interaction with N_2O can be estimated according to the concentrations and the reported rate constant of $k_{N_2O} = 1.16 \times 10^{-10}$ cm^3 molecule^{-1} s^{-1}.[11] Under the present conditions, the ratio of the contributions of $k_{N_2O}[N_2O]$ to $k_{CF_3CN}[CF_3CN]$ were less than 0.1. The plots of the reduced decay rate, *i.e.* $k - k_{N_2O}[N_2O]$, *vs.* the CF_3CN pressure are shown in Fig. 3, where both O(^{1}D) decay rate and O(^{3}P) rise rate data are included. The slope of the line determined by the least-squares fit with individual errors of the plotted values in Fig. 3 yields the rate constant k_{CF_3CN}. As can be seen in Fig. 3, the data of the O(^{1}D) decay rates and the O(^{3}P) rise rates are consistent. The value measured here was $k_{CF_3CN} = (1.3 \pm 0.2) \times 10^{-10}$ cm^3 molecule^{-1} s^{-1}. The uncertainty is estimated from the error of the least square fitting in Fig. 3. This rate constant value obtained for CF_3CN is 1.5 times larger than the value for CF_3Cl.[11] The total reaction rate constants of O(^{1}D) by the reactants CF_3CN, CF_3Cl and N_2 are summarized in Table 1.

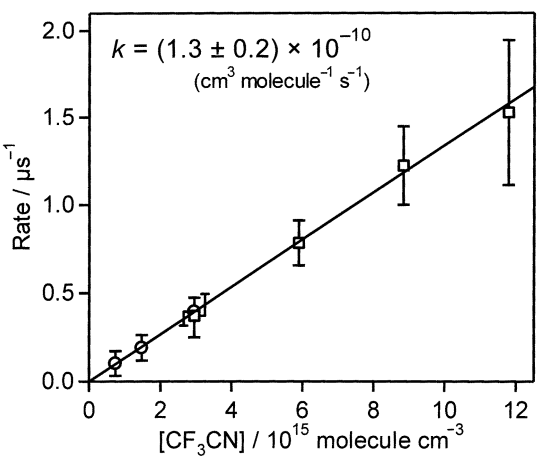

Fig. 3 Plot of the reduced $O(^1D)$ decay and $O(^3P)$ rise rates (see text) *vs.* the concentration of CF_3CN in the reaction cell. The rates were determined by analyzing the temporal profiles of the $O(^1D)$ signal (○) and of the $O(^3P)$ signal (□).

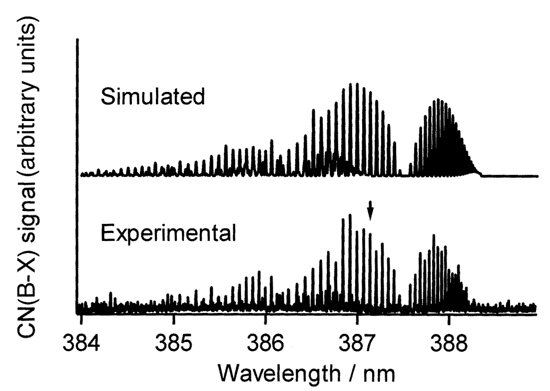

Fig. 4 LIF spectrum of the $CN(B\,^2\Sigma^+–X\,^2\Sigma^+)$ transition observed in the reaction between $O(^1D) + CF_3CN$ (lower trace) and simulated spectrum (upper trace) with vibrational and rotational temperatures of 3000 and 300 K, respectively. The delay time of the probe laser pulse is 15 µs after the photolysis laser pulse to produce $O(^1D)$. An arrow indicates the wavelength of the R(5) line of 0–0 transition for measuring the temporal profile of CN(X) in Fig. 5.

3.2. Quantum yield for the electronic quenching of $O(^1D)$

Since in the reaction with N_2 the $O(^1D)$ atom is quenched to $O(^3P)$ [eqn. (9)] with unit efficiency,[11] the asymptotic signal intensity measured in the reaction $O(^1D) + CF_3CN$ can be normalized by comparison with that in the reaction $O(^1D) + N_2$ under the same initial concentration of $O(^1D)$. The ratio obtained by this comparison is the quantum yield, ϕ_q, for the electronic quenching of $O(^1D)$. The $O(^3P_2)$ signal intensities for $O(^1D) + CF_3CN$ and $O(^1D) + N_2$ were compared at a delay of 15 µs when the $O(^3P_2)$ signals reached plateau levels and the reactions were completed. In the ϕ_q measurements, the partial pressures of CF_3CN and N_2 were determined so that the rise rates of the $O(^3P_2)$ signals had the almost identical values between the $O(^1D) + CF_3CN$ and $O(^1D) + N_2$ reaction systems. The pressures of CF_3CN and N_2 were 72 and 360 mTorr, and the total pressure with the He buffer gas was 2 Torr. The rise time of the $O(^3P_2)$ signals was about 0.3 µs^{-1}. Since the pressure of He buffer gas was 5 times higher than those of reactants (CF_3CN and N_2), hot atoms effects should be negligibly small. The value of ϕ_q measured thus was 0.14 ± 0.02, then the quenching rate constant, $k_q = k_{CF_3CN}\,\phi_q$, is calculated to be $(1.8 \pm 0.4) \times 10^{-11}$ cm^3 molecule^{-1} s^{-1}. The uncertainty of ϕ_q is estimated from the standard deviation (1σ) of five measurements and systematic errors.

3.3. $CN(X\,^2\Sigma^+)$ formation

The $CN(X\,^2\Sigma^+)$ radical products were observed in the reaction of $O(^1D)$ with CF_3CN. Fig. 4 shows the LIF excitation spectrum of the $CN(B\,^2\Sigma^+–X\,^2\Sigma^+)$ transition measured in the present reaction process at the delay time of 15 µs. The pressures of CF_3CN and N_2O were 45 and 10 mTorr, respectively, and the total pressure was 1 Torr with He buffer gas. The temporal profile of CN(X) with the excitation laser wavelength fixed at the R(5) line of the B–X 0–0 transition is shown in Fig. 5. The simulation spectrum in the upper part of Fig. 4 indicates that the CN(X) radicals are rotationally relaxed ($T_{rot} = 300$ K) but still vibrationally excited ($T_{vib} = 3000$ K) at a delay of 15 µs. The LIF spectrum of CN in Fig. 4 was taken in the plateau region of the time profile as shown in Fig. 5. The rotational relaxation rate should be faster than 1 µs^{-1} at the total pressure of 1 Torr. Therefore, the rise of the time profile shown in Fig. 5 reflects the reactive formation rate of the CN(X) radicals. The rise rate of this profile, *i.e.* 0.33 ± 0.07 µs^{-1}, is consistent with the $O(^1D)$ decay rate of 0.26 ± 0.04 µs^{-1} which is estimated from the reaction rates of $O(^1D) + CF_3CN$ and $O(^1D) + N_2O$ under the experimental conditions of Fig. 5. This suggests that the CN(X) radicals are produced by the direct reaction between $O(^1D)$ and CF_3CN, eqn. (7). Because no standard value of the quantum yield for the

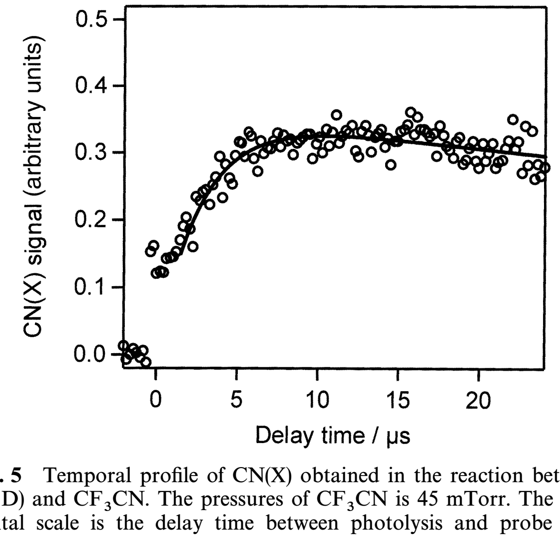

Fig. 5 Temporal profile of CN(X) obtained in the reaction between $O(^1D)$ and CF_3CN. The pressures of CF_3CN is 45 mTorr. The horizontal scale is the delay time between photolysis and probe laser pulses. The solid line is the least-squares fit to the observed profile by the rising function. The prominent signal at 0 µs is caused by scattered light from the photolysis laser used to produce $O(^1D)$.

Table 1 Total rate constants for the removal of $O(^1D)$, k_{total}, quantum yields for the electronic quenching of $O(^1D)$, ϕ_q, and calculated rate constants for the electronic quenching, $k_q = \phi_q\,k_{total}$, at room temperature

	$k_{total}/10^{-11}$ cm^3 molecule^{-1} s^{-1}	ϕ_q	$k_q/10^{-11}$ cm^3 molecule^{-1} s^{-1}	Ref.
CF_3CN	13 ± 2	0.14 ± 0.02	1.8 ± 0.4	This work
CF_3Cl	8.7	0.16 ± 0.05	1.4 ± 0.5	11, 5
N_2	2.6	1	2.6	11

CN(X) formation in the reaction of O(^{1}D) has been determined, the branching ratio for this reaction pathway of eqn. (7) was not measured.

3.4. NCO(X $^2\Pi$) formation

Fig. 6 shows the LIF excitation spectrum of the NCO(A $^2\Sigma^+$–X $^2\Pi$) transition measured at a delay time of 100 μs after the irradiation of 193 nm laser pulse to the $N_2O + CF_3CN$ gas mixture in the cell. The NCO(X $^2\Pi$) and NCO(A $^2\Sigma^+$) radicals were not observed in the reaction of O(^{1}D) with CF_3CN on the same time scale as the production of O(^{3}P) and CN(X) productions. The temporal profile of NCO(X) in the vibrationally ground state was measured as shown in Fig. 7. No significant signals of the vibrationally excited NCO(X) were detected in the present study. The NCO(X $^2\Pi_{3/2}$) and NCO(X $^2\Pi_{1/2}$) radicals were detected by LIF signal at the Q_1 and P_2 band-heads of the A $^2\Sigma^+$–X $^2\Pi$ transition, respectively.[15] The LIF signal intensity did not reach an asymptotic value until the delay time of *ca.* 100 μs for a CF_3CN pressure of 45 mTorr. This temporal profile was almost independent of the N_2O concentration. Since this time scale is much larger than that of production rates of O(^{3}P) and CN(X), the NCO(X) radical is not formed by the primary process of O(^{1}D) + CF_3CN.

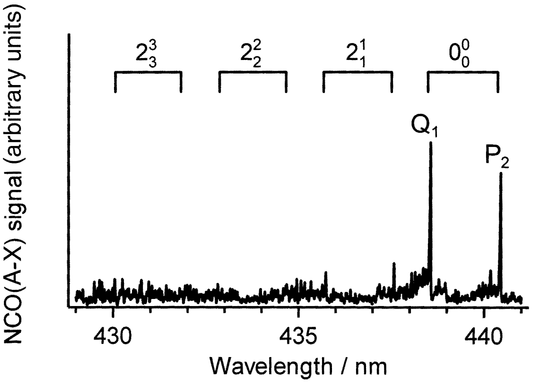

Fig. 6 LIF spectrum of the NCO(A $^2\Sigma^+$–X $^2\Pi$) transition observed in the present study. The delay time of the probe laser pulse is 100 μs after the photolysis laser pulse to produce O(^{1}D). The Q_1 and P_2 band-heads of the 0–0 ($K = 1$) transition indicated over the peaks were used for measuring the temporal profiles of NCO(X) in Fig. 7. The other strong Q_1 and P_2 band-heads expected to appear as hot-band transitions for each bending quantum number v_2 ($K = v_2 + 1$) are also marked, but are not present.

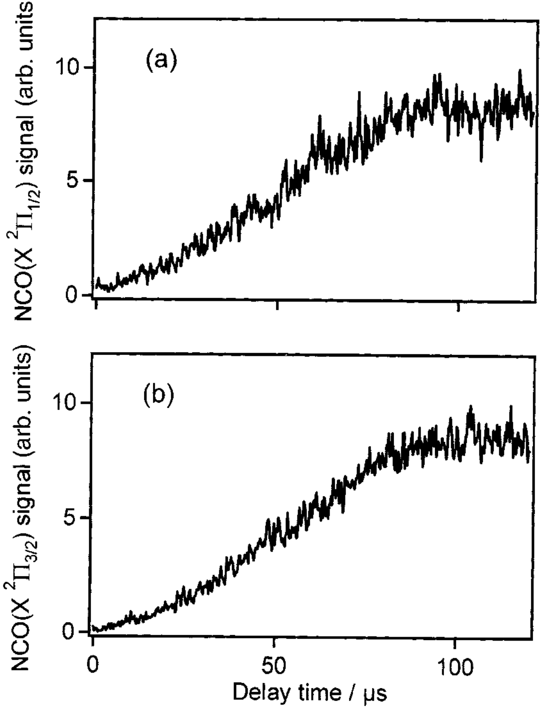

Fig. 7 Temporal profile of NCO(X) obtained by monitoring LIF intensities of the (a) P_2 and (b) Q_1 band-heads of NCO(A $^2\Sigma^+$–X $^2\Pi$, 0–0) transitions. The pressures of CF_3CN are 45 mTorr. The horizontal scale is the delay time between photolysis and probe laser pulses.

4. Discussion

4.1. Electronic quenching process

The CF_3CN molecule was used as a surrogate for CF_3Cl. In the case of the reaction between CF_3Cl and O(^{1}D), it is supposed that the approach of O(^{1}D) toward the F end of CF_3Cl is not effective in the quenching process.[5] That is suggested by the fact that the CF_4 molecule is quite inert to quenching of O(^{1}D). The quenching rate constant for CF_4 is 2×10^{-14} cm^3 molecule^{-1} s^{-1}.[11] Addison has suggested[16] that the attractive interaction is effective between the vacant p-orbital of O(^{1}D) and the lone-pair on the Cl atom end. On the other hand, molecular orbitals for the CN end in the CF_3CN molecule are similar to those of N_2 molecule by which the electronic quenching process of O(^{1}D) is well known.[17–19] The interaction of O(^{1}D) with the CN end is expected to be strong enough to form stable CF_3CNO species as well as that from the interaction of O(^{1}D) with N_2 forms the N_2O molecule. The quenching rate constants of O(^{1}D) by the reactants CF_3CN, CF_3Cl and N_2 are summarized in Table 1. In the mechanism of quenching process by N_2, the reaction proceeds via the collision complex N_2O as an intermediate.[14] The O(^{1}D) atom approaches the N_2 molecule on the potential energy surface (PES) of $N_2O(^1A')$ leading from $N_2O(X\,^1\Sigma^+)$ to $N_2(X\,^1\Sigma_g^+)$ + O(^{1}D). This singlet PES crosses the triplet PESs of $N_2O(^3A')$ and $N_2O(^3A'')$ to form the $N_2(X\,^1\Sigma_g^+)$ and O(^{3}P) products at an N–O distance of *ca.* 0.19 nm.[18] The collision complex can decompose to N_2 + O(^{3}P) through the crossing seam between these singlet and triplet PESs.

In the present case of the quenching process by CF_3CN, the O(^{1}D) atom can approach the N end on the singlet PES leading to $CF_3CNO(S_0)$. The triplet PES of $CF_3CNO(T_1)$ correlating to CF_3CN + O(^{3}P) intersects this singlet PES. At the seam of the intersection the intersystem crossing, *i.e.* $S_0 \rightarrow T_1$, should occur. Therefore it is proposed that the CF_3CNO intermediate is formed in the quenching reaction process.

4.2. CN(X $^2\Sigma^+$) production process

The mechanism of the similar reaction system O(^{1}D) + HCN should provide us with useful information about the reaction O(^{1}D) + CF_3CN. The reaction of O(^{1}D) with HCN has been studied by Carpenter *et al.*[20] and Kreher *et al.*[21] The main pathway of this reaction is

$$HCN + O(^1D) \rightarrow NH(a\,^1\Delta) + CO(X\,^1\Sigma^+); \quad -\Delta H = 195 \text{ kJ mol}^{-1}, \quad (11)$$

and other dominant pathway is

$$HCN + O(^1D) \rightarrow OH(X\,^2\Pi) + CN(X\,^2\Sigma^+); \quad -\Delta H = 100 \text{ kJ mol}^{-1}. \quad (12)$$

The reaction channel of eqn. (12) can proceed through both the direct H atom elimination process by O(^{1}D) and the insertion process forming the HOCN intermediate. Kreher *et al.*

suggested[21] the reaction mechanism for the production of $CN(X\,^2\Sigma^+)$, in which formation of the intermediates $HOCN(X\,^1A')$ and/or $HOCN(A\,^1A'')$ followed by decomposition into the products $OH(X\,^2\Pi) + CN(X\,^2\Sigma^+)$ occur by the direct insertion of $O(^1D)$ into the H–C bond or the insertion process through the cyclic H–(CNO), *viz.*

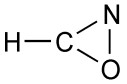

Based on the foregoing discussion, it is expected that the cyclic CF_3–(CNO) intermediate, *viz.*

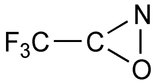

could be formed in the reaction between $O(^1D)$ and CF_3CN. The highly excited vibrational energy of the cyclic intermediate CF_3–(CNO) is not sufficient to cleave the C–C bond, *i.e.* to produce the cyclic (CNO) radical, but is sufficient for isomerization to form CF_3OCN^* which dissociates to the products $CF_3O + CN(X\,^2\Sigma^+)$. Anyway, observing CN products in the present study, we conclude that the insertion process forming the CF_3–O–(CN) intermediate occurs in the reaction of $O(^1D) + CF_3CN$.

As described before, the coincidence between the CN(X) signal rise rate and the estimated reaction rate of $O(^1D) + CF_3CN$ suggests that the CN radicals are produced by direct reaction between $O(^1D)$ and CF_3CN, eqn. (7). Another candidate for the CN(X) formation path is decay from the electronic excited state CN(A) produced by eqn. (8). The radiative rate of CN(A) is *ca.* 0.15 μs^{-1} which is much slower than the rise time of the CN(X) signal. The electronic quenching rates of CN(A) by collisions with various gas molecules were reported to be in the range $(0.5 \sim 11) \times 10^{11}$ cm^3 $molecule^{-1}$ s^{-1}.[22] However, the quenching rate of CN(A) is unknown under our experimental conditions. Thus, the possibility of the formation of CN(X) from CN(A) cannot be omitted.

4.3. Source of $NCO(X\,^2\Pi)$ radical

In the present reaction of $CF_3CN + O(^1D)$, the $NCO(X\,^2\Pi)$ radical is not produced on the time scale of the reactions which produce $O(^3P)$ and CN(X) productions. Carpenter *et al.*[20] observed LIF of NCO radicals in the reaction of $O(^1D) + HCN$. They also reported that the production process of NCO has a slow rise time and concluded that the NCO radicals were not primary products of $O(^1D) + HCN$. There are several possible processes which are responsible for the slow NCO formation. One may be a secondary reaction of the primary $O(^3P)$ products, *i.e.* $O(^3P) + CF_3CN$, or CN products, *i.e.* $CN + O(^1D/^3P)$ and $CN + N_2O$. Another is the collision-induced decomposition process of the long-lived intermediate $(CF_3CN–O)^*$ produced by the reaction of $O(^1D) + CF_3CN$, *i.e.*

$$CF_3CN + O(^1D) \rightarrow (CF_3CN\text{–}O)^*, \qquad (13)$$

$$(CF_3CN\text{–}O)^* + CF_3CN \rightarrow CF_3CN + CF_3 + NCO(X\,^2\Pi). \qquad (14)$$

The reaction of $O(^3P)$ is expected to be slow, since the rate constant of the similar reaction,

$$HCN + O(^3P) \rightarrow \text{Products}, \qquad (15)$$

is very slow, *i.e.* $k = 1.5 \times 10^{-17}$ cm^3 $molecule^{-1}$ s^{-1} at 298 K.[11] It was suggested that all the reaction coordinates of $HCN + O(^3P)$ have energy barriers.[16,23] It was found in our experiments that the rise rates of the NCO LIF signal were not affected at all by increases in the N_2O concentration, that is the concentration of $O(^1D)$. This means that the $NCO(X\,^2\Pi)$ product is unlikely to be formed by the reaction of the primary reaction products such as CN and $O(^3P)$. Therefore, we suggest NCO formation by reactions (13) and (14). However, further experiments are required to elucidate the formation process of the NCO radical.

5. Summary

The reaction processes of CF_3CN with $O(^1D)$ were studied using the time-resolved LIF detection of $O(^3P)$, $O(^1D)$, CN(X) and NCO(X). CF_3CN can be regarded as a pseudo-CF_3Cl molecule. The total rate constant between $O(^1D)$ and CF_3CN was measured to be $(1.3 \pm 0.2) \times 10^{-10}$ cm^3 $molecule^{-1}$ s^{-1} at room temperature. This value is 1.5 times faster than the rate constant for the reaction of CF_3Cl with $O(^1D)$. The quantum yield of the electronic quenching process, ϕ_q, was determined by comparison with the reaction of $N_2 + O(^1D)$. The value of ϕ_q was measured to be 0.14 ± 0.02 for $O(^1D) + CF_3CN$, which is almost identical with that for $O(^1D) + CF_3Cl$. The CN radical was observed as a primary product in the reaction of $O(^1D) + CF_3CN$. The insertion process forming the CF_3–O–(CN) intermediate may occur in this reaction, which results in the formation of CN. Since the rise rates of the LIF signal of the $NCO(X\,^2\Pi)$ radical were much slower than the total reaction rates of $O(^1D) + CF_3CN$, it is concluded that the $NCO(X\,^2\Pi)$ radical is not a primary product.

Acknowledgements

Support of this work by Grants-in-Aid from the Ministry of Education, Science and Culture, is acknowledged. This work was partly supported by the research project, "Computational chemistry for atmospheric environmental molecule" under Research and Development Applying Advance Computational Science and Technology administrated by Japan Science and Technology Corporation (ACT-JST).

References

1 R. J. Cvetanović, *Can. J. Chem.*, 1974, **52**, 1452.
2 A. R. Ravishankara, S. Solomon, A. A. Turnipseed and R. F. Warren, *Science*, 1993, **259**, 194.
3 B. J. Finlayson-Pitts and J. N. Pitts, Jr., *Chemistry of the Upper and Lower Atmosphere: Theory, Experiments and Applications*, Academic Press, San Diego, 1999.
4 G. P. Brasseur, J. J. Orlando and S. S. Tyndall, *Atmospheric Chemistry and global change*, Oxford University Press, London, 1999.
5 K. Takahashi, R. Wada, Y. Matsumi and M. Kawasaki, *J. Phys. Chem.*, 1996, **100**, 10145.
6 A. P. Force and J. R. Wiesenfeld, *Phys. Chem.*, 1981, **85**, 782.
7 M. J. Molina and F. S. Rowland, *Nature*, 1974, **249**, 810.
8 F. S. Rowland and M. J. Molina, *Rev. Geophys. Space Phys.*, 1975, **13**, 1.
9 World Meteorological Organization, *Scientific Assessment of Ozone Depletion: 1998*, Global Ozone Research and monitoring project, Report No. 44, 1998.
10 M. W. Chase, *NIST-JANAF Thermochemical Tables, 4th edition*, *J. Phys. Chem. Ref. Data*, Monograph 9, 1998.
11 W. B. DeMore, S. P. Sander, D. M. Golden, R. F. Hampson, M. J. Kurylo, C. J. Howard, A. R. Ravishankara, C. E. Kolb and M. J. Molina, *Chemical Kinetics and Photochemical Data for Use in Stratospheric Modeling*, NASA, JPL Publ. 97-4, Pasadena, 1997.
12 M. Abe, Y. Sato, Y. Inagaki, Y. Matsumi and M. Kawasaki, *J. Chem. Phys.*, 1994, **101**, 5647.
13 Y. Matsumi, S. M. Shamsuddin, Y. Sato and M. Kawasaki, *J. Chem. Phys.*, 1994, **101**, 9610.
14 L. J. Stief, W. A. Payne and R. B. Klemm, *J. Chem. Phys.*, 1975, **62**, 4000.
15 D. Patel-Misra, D. G. Sauder and P. J. Dagdigian, *J. Chem. Phys.*, 1990, **93**, 5448.

16 A. M. Mebel, A. Luna, M. C. Lin and K. Morakuma, *J. Chem. Phys.*, 1996, **105**, 6439.
17 J. C. Tully, *J. Chem. Phys.*, 1974, **61**, 61.
18 H. Tachikawa, T. Hamabayashi and H. Yoshida, *J. Phys. Chem.*, 1995, **99**, 16630.
19 Y. Matsumi and A. M. S. Chowdhury, *J. Chem. Phys.*, 1996, **104**, 7036.
20 B. K. Carpenter, N. Goldstein, A. Kam and J. R. Wiesenfeld, *J. Chem. Phys.*, 1984, **81**, 1785.
21 C. Kreher, R. Theinl and K.-H. Gericke, *J. Chem. Phys.*, 1995, **103**, 8901.
22 Y. Huang, R. Lu and J. B. Halpern, *Appl. Opt.*, 1993, **32**, 981.
23 N. Marchand, P. Jimeno, J. C. Rayez and D. Liotard, *J. Phys. Chem. A*, 1997, **101**, 6077.